Polymer Bulletin (2023) 80:4035–4059
https://doi.org/10.1007/s00289-022-04238-7

ORIGINAL PAPER

Synthesis, characterization, anticancer, and antioxidant activities of chitosan Schiff bases bearing quinolinone or pyranoquinolinone and their silver nanoparticles derivatives

Mai A. Mostafa[1] · Mostafa M. Ismail[1] · Jehan M. Morsy[1] · Hany M. Hassanin[1] · Marwa M. Abdelrazek[1]

Received: 5 August 2021 / Revised: 17 October 2021 / Accepted: 11 April 2022 /
Published online: 9 May 2022

Abstract

In this work, new chitosan-based Schiff bases were synthesized by the reaction of chitosan with quinolinone and pyranoquinolinone giving **CSQ**, and **CSP**, respectively. The novel Chitosan Schiff bases were grafted on silver nanoparticles providing **CSQ/Ag**, **CSP/Ag** structures. Characterization of isolated compounds was carried out by FT-IR, TGA, XRD, SEM, and TEM. The target compounds **CSQ**, **CSP**, **CSQ/Ag**, and **CSP/Ag** were evaluated as antitumor agents against three cancer cell lines, liver (HepG-2), colon (HCT-116), and breast (MCF-7). Compound **CSQ/Ag** disclosed potent cytotoxic effect with IC_{50} values in the range of 41.9–55.1 µg/ml in comparison with 5-fluorouracil against different cancer cell lines. Besides, the antioxidant activity of chitosan and its quinolinone and pyranoquinolinone analogues was assessed as radical scavengers versus 1,1-diphenyl-2-picrylhydrazyl radicals (DPPH%). The compound **CSQ/Ag** emerged as the most active member in scavenging the DPPH radicals. The obtained findings proved that the new Schiff bases/silver nanoparticles of chitosan showed higher antiproliferative and antioxidant activities than the blank **CS** and would be highly applicable in biomedical fields.

✉ Mai A. Mostafa
maiabdellatef@edu.asu.edu.eg

[1] Department of Chemistry, Faculty of Education, Ain Shams University Roxy, Cairo 11711, Egypt

Graphical abstract

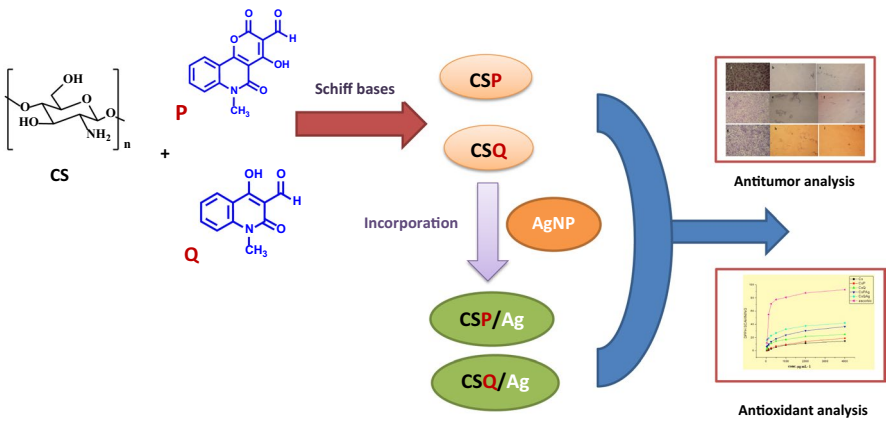

Keywords Chitosan Schiff bases · Quinolinone · Pyranoquinolinone · Antitumor · Cell line · Antioxidant

Introduction

Chitosan is a more useful form of chitin and the second most abundant biopolymer in nature that forms most of the exoskeleton of crustaceans [1]. It is one of the most utilized polymers in pharmaceutical research [2, 3]. Chitosan and its crosslinked grafts have obtained remarkable significance in the field of therapeutic applications like drug delivery, enzyme immobilization, tissue engineering, and pH-sensitive protein carriage [4, 5] due to its exclusive features such as biodegradability, biocompatibility, non-toxicity, and non-immunogenicity [6]. Furthermore, chitosan derivatives have exhibited antimicrobial activity [7] and anticancer activity with minimal toxicity on noncancer cells, such activity against various cancer cell lines significantly depends upon molecular weight and degree of deacetylation affected by the distribution pattern of β-(1,4)-linked N-acetylglucosamine and D-glucosamine units along the oligomeric chain [8]. Chitosan is informed as an important antioxidant agent and, therefore, could be used as an alternative to synthetic antioxidants such as butylated hydroxy-anisole (BHA), butylated hydroxytoluene (BHT), and tert-butylhydroquinone (TBHQ) [9–11].

Otherwise, quinolines are distinct moieties existing in diverse biologically active natural or synthetic compounds. They have been widely utilized for the synthesis of various drugs depicted for several diseases. Quinoline skeleton executes numerous pharmaceutical applications such as antibacterial, antitumor, antifungal, anti-inflammatory, analgesic, and antimalarial [12, 13].

Pyranoquinolinone is of considerable interest as it is a core structure in a number of alkaloids that discloses cancer cell inhibitory activity and is regarded

as a potential antitumor agent [14, 15]. The substances containing pyrano[3,2-*c*] quinoline moiety show powerful anti-proliferative effects against distinctive cell lines [16–18]. Additionally, many pyrano[3,2-*c*]quinolinone scaffolds possess good antioxidant activity and would be promising antioxidant agents [19, 20].

On the other hand, Schiff bases of heterocyclic rings are well known due to their broad range of applications in biological and industrial fields [21]. They are distinguished by the presence of the azomethine linkage which is responsible for a broad spectrum of bioactivities. Schiff bases compounds have been shown to have promising results on breast carcinoma cell line [22]. Furthermore, some Schiff base derivatives exhibit potential as anticancer drugs across five cell lines (HeLa, HCT-116, MCF-7, HepG-2, and HL-60 cells) [23, 24]. A series of compounds-based Schiff bases are reported to be excellent radical scavengers and act as antioxidant agents [25, 26]. Additionally, some pyranoquinolinone-based Schiff's have received noticeable TOP2B inhibitory activity against breast cancer cell line (MCF-7) compared to the drug doxorubicin [27]. Moreover, Chitosan anchored Schiff bases have received intensive interest for their better-expanded bio-functional properties than the parent chitosan itself such as antibacterial, antitumor, and antioxidant activities [28, 29].

Meanwhile, several nanocomposites containing metal, and metal oxide nanoparticles, graphene, and inorganic clays manifest recent applications in industrial, biomedical engineering, wastewater treatment, and agricultural fields [30, 31] such as notable inhibitory activity against some bacterial strains like E.coli and S.aureus [32, 33] and high-performance capacitors in the field of energy storage [34]. More concretely, silver nanoparticles have obtained much interest in the Nanomedicine fields. Many mechanisms have been hypothetically proposed for their activity such as antioxidant protection, enhanced carcinogen detoxification, inhibitory activity of tumor cells, surveillance of immune enhancement, inhibition of angiogenesis, and modeling of cell proliferation [35]. Modern studies have also revealed that Ag NPs possess considerable anticancer activity and have significant ability to stimulate cytotoxicity in cancer cells through different mechanisms including DNA damage, oxidative stress, cell cycle arrest, necrosis, or apoptosis [36]. Interestingly, chitosan which is decorated with silver nanocomposites reveals promising antimicrobial, antitumor, antimycobacterial, electrical resistance, and flame retardancy [37–41].

The versatile chemotherapeutical activities of chitosan and Schiff bases as well as the quinolinones and pyranoquinolinones systems mentioned above inspired us to generate novel Schiff base holding quinolinone and chitosan in one framework and another Schiff base containing pyrano[3,2-*c*]quinolinone and chitosan analogs embedded in one skeleton which can be utilized as valuable substructures for improvement their pharmacological properties and exploration new anticancer chemotherapeutics and antioxidant drugs. Likewise, we have incorporated silver nanoparticles to the new synthesized Schiff bases, hoping that the produced compounds will be eco-friendly promising pharmaceutical candidates. As well, we describe their promising inhibitory activity against cancer cells proliferation and examine their antioxidant activity.

Results and discussion

Ag nanoparticles characterization

The crystal structure of synthesized silver nanoparticles was examined using XRD analysis. The four different diffraction peaks of 31, 46, 67, and 78 were pointing to planes (111), (200), (220), and (311), respectively. The planes signified that the Ag NPs are face-centered cubic structured (JCPDS 89-3722) [42, 43]. The results of the diffraction pattern are illustrated in Fig. 1 corresponding to pure silver metal powder. The crystallite size (d) was estimated by Debye–Scherer's equation as follows:

$$d = k\lambda = \beta \cos\theta$$

where, K is the shape factor between 0.9 and 1.1, λ is the incident X-ray wavelength (Cu $K_\alpha = 0.154$ nm), β is the full width at half maximum and Θ is the position of that line in the pattern [44]. The average crystallite size of Ag NBs is $d = 14$ nm. The TEM image (Fig. 1b) indicates that the shape and size of the Ag NPs are spherical and nanoscale, respectively [45].

Synthesis route of the novel chitosan Schiff bases CSP and CSQ

Scheme 1 illustrates the reaction of chitosan with 3-formylquinolinone **Q** or 3-formylpyranoquinolinone **P** via Schiff base condensation reaction. Chitosan amino group and aldehydic group of **Q** or **P** reacted by nucleophilic attack forming azomethine group.

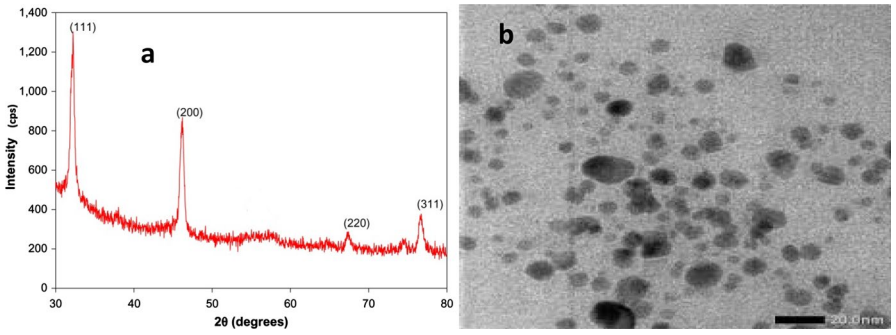

Fig. 1 Ag NPs characterization; **a** XRD and **b** TEM

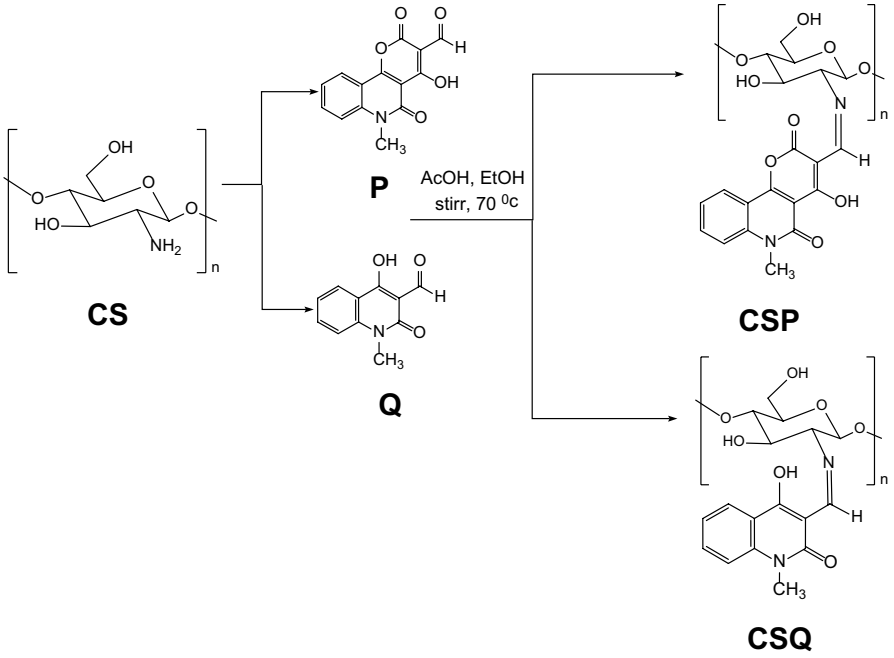

Scheme 1 Formation of chitosan Schiff bases **CSP** and **CSQ**

Characterization of the prepared chitosan Schiff bases and their silver nanocomposites

FT-IR spectra

The chitosan Schiff base **CSP** was prepared and characterized by the method reported by Ibrahim et al. [46]. The comparative structural conformation of **CS**, **CSQ**, **CSP**, **CSQ/Ag**, and **CSP/Ag** membranes were verified from the characteristic transmittance peaks of the IR spectrum (Fig. 2). The spectrum of pure chitosan proved the appearance of overlapped characteristic absorption stretching vibrations between O–H and N–H at 3431 cm^{-1}, in addition to the presence of two peaks at 2919 and 2866 cm^{-1} due to C–H. Three new stretching bands of NH, CH_3, and the second hydroxyl group (OH) appear at 1619, 1466, and 1389 cm^{-1}, respectively. In comparison to the IR spectrum of chitosan, the IR spectra of chitosan Schiff bases **CSQ** and **CSP** showed the appearance of new peaks at 1652 (C = O quinolone) for **CSQ**, and at 1748 (C = O α-pyrone), 1678 (C = O quinolone) for **CSP**, in addition to the broad band at 3400 cm^{-1} in **CSQ**, and at 3424 cm^{-1} in **CSP** corresponding to N–H and O–H. Besides, a strong new peak appeared at 1604 for **CSQ** and at 1634 cm^{-1} in **CSP** assigned to the characteristic absorbance of azomethine group (C = N), confirming the formation of chitosan Schiff bases [47]. The peaks observed around 1530 cm^{-1} were attributed to the N–H bending in secondary amides (amide II band) in **CSQ** and **CSP**. Furthermore, the IR spectra of **CSQ** and **CSP** displayed

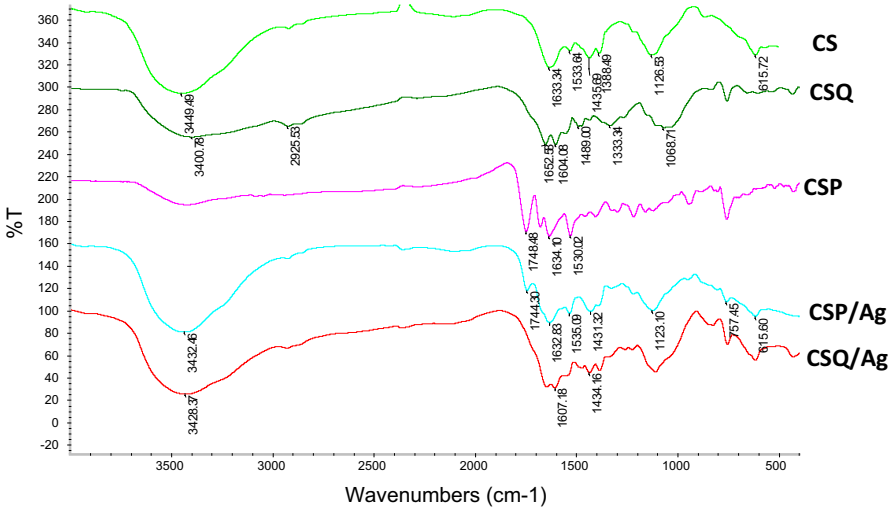

Fig. 2 FT-IR spectra of pure chitosan **CS**, Schiff bases **CSQ, CSP** and Schiff basses capped AgNPs **CSQ/Ag**, **CSP/Ag**

absorption bands around 1450 and 840 cm^{-1} due to OH in-plane bending, and the presence of symmetrical C-H bending in CH_3 around 1161 cm^{-1}. Two notable peaks around 1020 cm^{-1} and around 1221 cm^{-1} are characteristic for C–O–C bridge stretching, and C-O stretching vibration, respectively [48].

The FT-IR spectra of the prepared silver nanocomposites **CSQ/Ag** and **CSP/Ag** were also compared with that of **CSQ** and **CSP**, respectively, to investigate the possible functional groups of **CSQ** and **CSP** responsible for the reduction and stabilization of Ag NPs. The change of some IR signatures coupled with the appearance of new ones and energy-shifts for some stretching vibrations in the FTIR spectra of **CSQ/Ag** and **CSP/Ag** as compared with that of **CSQ** and **CSP**, respectively, confirms a successful capping of Ag NPs by **CSQ** and **CSP** (Fig. 2). Primarily, the broadness of the bands characteristic for the OH stretching vibrations along with their positive shift to 3428 and 3432 cm^{-1} for **CSQ/Ag** and **CSP/Ag**, respectively, in comparison to that of **CSQ** (3400 cm^{-1}) and **CSP** (3424 cm^{-1}), indicating the crucial role of OH groups in the reduction and stabilization of Ag NPs. Meanwhile, it was notable that the phenolic C–O group which appeared around 1221 cm^{-1} in **CSQ** and **CSP** disappeared completely in **CSQ/Ag** and **CSP/Ag**, confirming the participation of phenolic hydroxyl groups in the reduction and stabilization of Ag NPs. Interestingly, new peaks in the spectra of **CSQ/Ag** and **CSP/Ag** occurred at 1431 and 1434, respectively, distinctive for Ag NPs. All the previous differences prove the successful capping of Ag NPs with **CSQ** and **CSP** [49, 50].

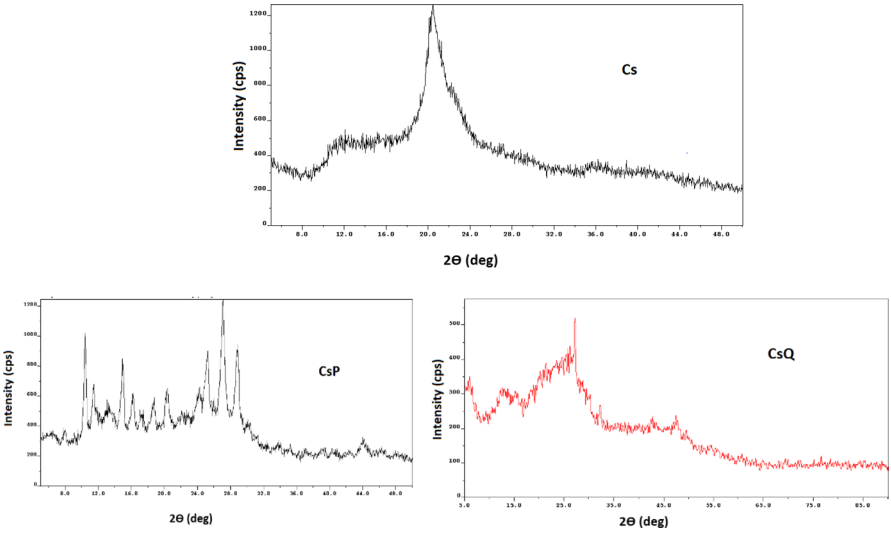

Fig. 3 X-ray diffraction patterns of **CS, CSQ** and **CSP**

X-Ray diffraction (XRD) study

The XRD spectra have been accomplished to analyze the crystalline structure of the synthesized membranes **CS**, **CSQ**, and **CSP** (Fig. 3). The chitosan sample exhibited a sharp peak at $2\theta = 20.4^{\circ}$ compatible with the previous studies [51]. This recommends the formation of intermolecular and intramolecular hydrogen bonds due to the presence of free amino groups in chitosan [52]. In the XRD patterns of **CSQ**, the intensity of the peak at 2θ of 20.4° decreased and becomes broader comparing with free chitosan; this reflects that the chitosan-quinolinone derivative has a less crystalline and more amorphous structure. This can be primarily due to the deformation of the strong hydrogen bonding in the chitosan backbone because of substitution of quinolinone on the N-atom of chitosan which causes the steric hindrance after Schiff base formation [53, 54]. According to the literature, the XRD of **CSP** showed depression in intensity and deformation of chitosan peak which at 2Θ of 20.4°, confirming the deformation of chitosan crystallinity. In addition, there was higher semicrystalline nature for **CSP** designating that there was molecular miscibility and as a result of Schiff base crosslinking between chitosan and the pyranoquinolinone moiety [46]. A comparative figure for XRD patterns of **CS**, **CSQ**, and **CSP** is delineated in Fig. 4.

Figure 5 reveals the X-ray diffraction of **CSP/Ag** and **CSQ/Ag**. The sharp peaks located at 2θ angles of 38°, 44.2°, 64.5°, and 77° in **CSP/Ag** were attributed to (111), (200), (220), and (311) planes of face-centered cubic Ag nanoparticles which confirms the silver reference file of JCPDF 03-065-287. While XRD patterns of **CSQ/Ag** disclosed the intense diffraction peaks at 2θ angles of 38°,

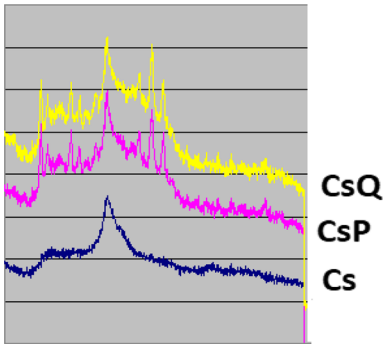

Fig. 4 Comparative figure of XRD patterns of **CS**, **CSP**, and **CSQ**

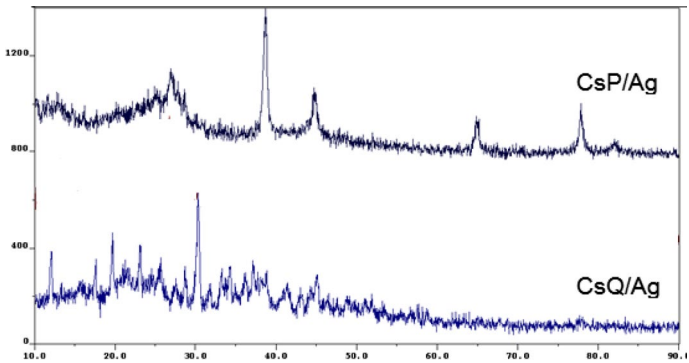

Fig. 5 X-Ray diffraction patterns of chitosan and CSBs with 1% silver nanoparticles

44.2° [55–57]. Such data approve the successful reduction in silver cations on the surface of chitosan Schiff bases **CSQ** and **CSP**.

Thermal gravimetric analysis (TGA)

Thermogravimetric analysis is employed to study the thermal stability behavior of the newly synthesized compounds as depicted in Fig. 6. Chitosan showed a total weight loss at 281 °C, corresponding to chitosan moiety, while in chitosan Schiff bases **CSQ** and **CSP**, the weight loss was observed at 322.55 °C and 343.05 °C, respectively. The observed temperature difference might be owing to the formation of chitosan Schiff bases. The outcomes verified the higher stability of chitosan Schiff bases at higher temperatures. The TGA curve of **CSQ/Ag** revealed a total loss in weight at 340 °C, illustrating the higher stability of **CSQ/Ag** as compared to **CSQ**. This displays the enhanced thermal stability owing to grafting on silver nanoparticles.

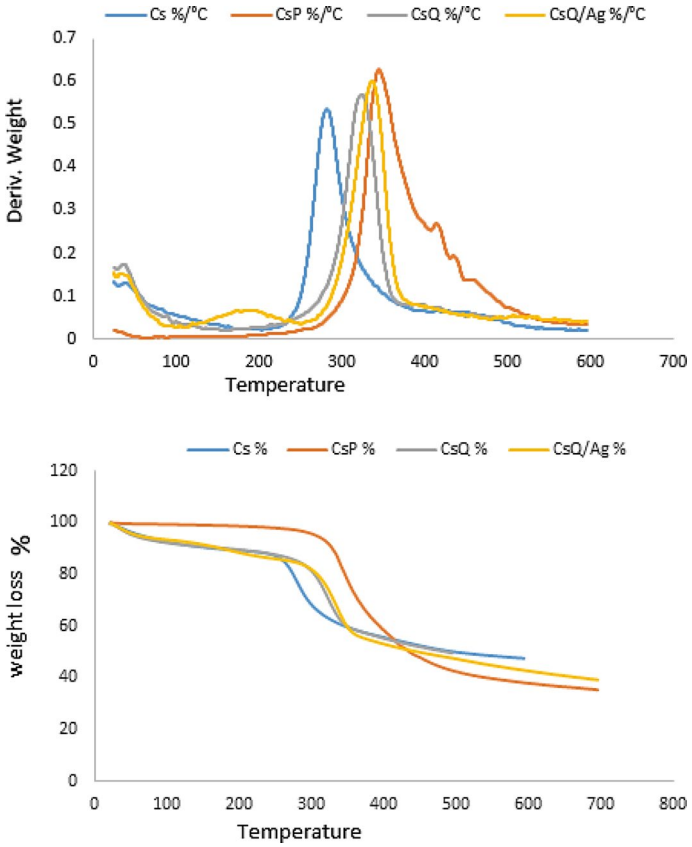

Fig. 6 TG curves of **CS**, **CSQ**, **CSP**, and **CSQ/Ag**

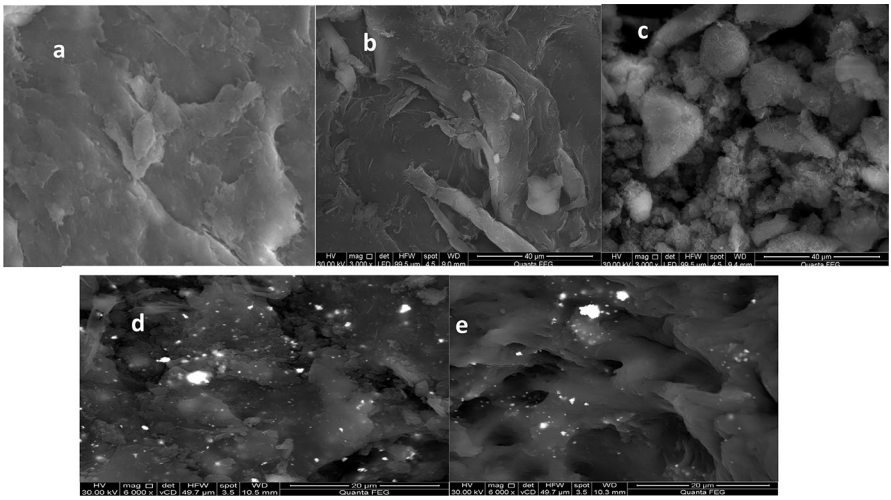

Fig. 7 SEM images of **a CS**, **b CSQ**, **c CSP**, **d CSQ/Ag**, **e CSP/Ag**

Scanning electron microscopy (SEM)

The SEM micrographs of CS, CS-Schiff's bases, and their silver nanocomposites are displayed in Fig. 7. It is clearly seen that the pure chitosan had a nonporous and smooth membranous surface (Fig. 7a), whereas **CSQ** and **CSP** revealed a significant surface roughness and porous surface [58] (Fig. 7b, c). The roughness could be attributed to the loss of hydrogen bonding of chitosan chains, depicting the successful modification of chitosan surface [59]. Moreover, grafting of bulky group (quinolinone or pyranoquinolinone) into chitosan polymer matrices gives a surface roughness [60]. By comparing SEM images in Fig. 7b, c of **CSQ** and **CSP** with Fig. 7d, e of **CSQ/Ag** and **CSP/Ag**, it is obvious that Ag NPs were mostly incorporated uniformly into **CSQ** and **CSP** matrix. This was assured by EDX (Fig. 8) which demonstrated the existence of elemental silver peaks in region of 3 keV. In addition, we noticed that the intensity of EDX peak of Ag NPs of **CSP/Ag** is greater than the one of **CSQ/Ag** [29]. Figure 7d, e signifies the well-dispersion of spherical shape of Ag NPs on the surface of **CSBs**, confirming that successful preparation of the **CSBs/Ag**. Interestingly, there is a good interaction between Ag NPs and **CSP**, while dispersion of Ag NPs in case of **CSQ** was to lower extent. This may be due to the activity of 4-OH group of quinolinone that assist in reducing and stabilizing silver nanoparticles [29, 56].

Transmission electron microscopy (TEM) of CSP/Ag and CSQ/Ag

TEM analysis of **CSP/Ag** and **CSQ/Ag** was performed and graphically drawn through histograms presented in Fig. 9. They revealed a moderate dispersion of Ag NPs into **CSP** and **CSQ** matrix besides some aggregates. Both images contain transparent central areas with dense dots representing the loaded silver nanoparticles into the CSBs matrix. The continuous spreading of the black spots in the Schiff bases proved the successful deposition of silver nanoparticles into the polymeric structure. Semi-spherical Ag NPs are observed with an average size of 30–50 nm.

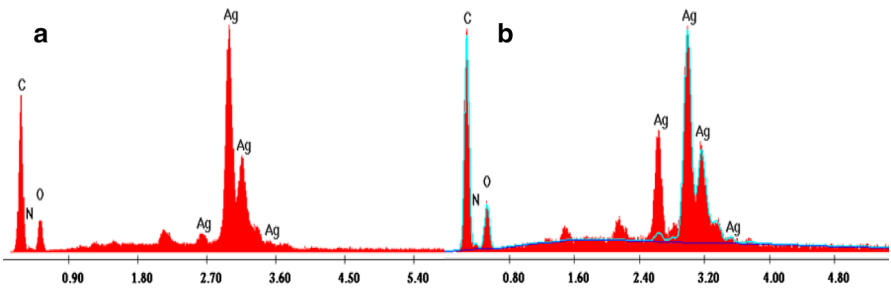

Fig. 8 EDX of **a CSP/Ag** and **b CSQ/Ag**

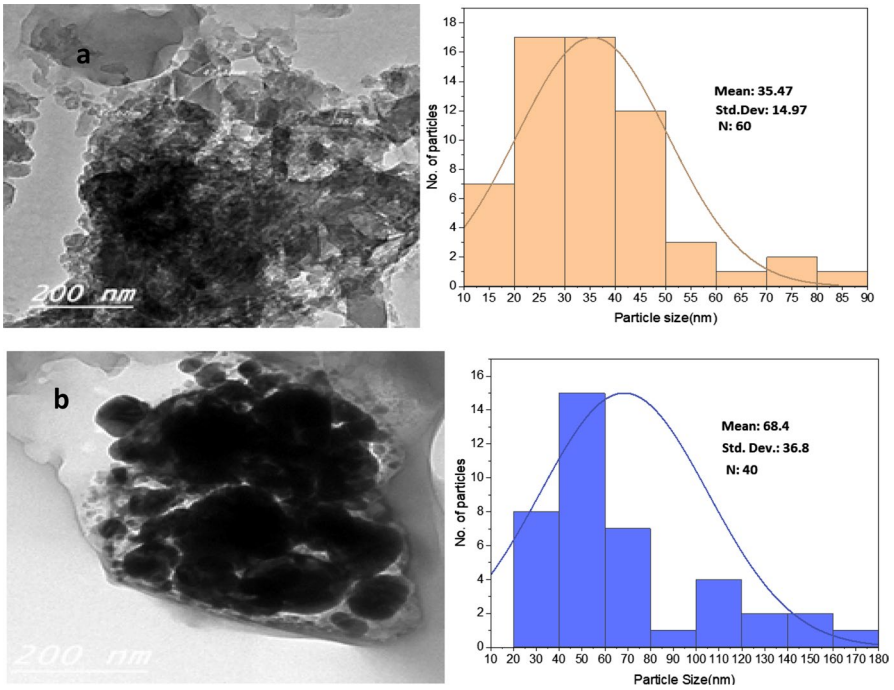

Fig. 9 TEM images of **a CSP/Ag** and **b CSQ/Ag** with related histograms

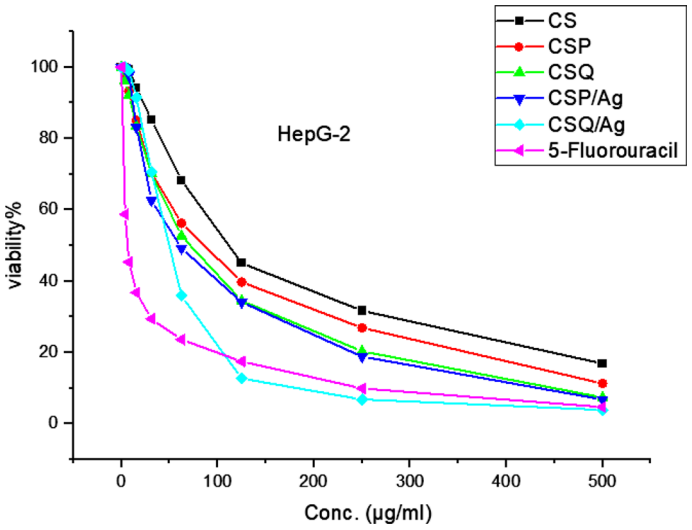

Fig. 10 Effect of concentration (0–500 µg/ml) of compounds **CS**, **CSQ**, **CSP**, **CSQ/Ag**, **CSP/Ag**, and 5-fluorouracil on viability of human liver cancer (HepG-2) cell line

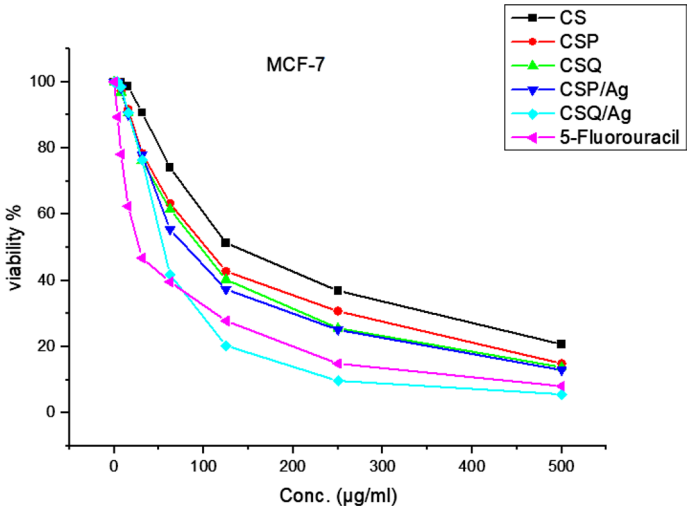

Fig. 11 Effect of concentration (0–500 µg/ml) of compounds **CS**, **CSQ**, **CSP**, **CSQ/Ag**, **CSP/Ag**, and 5-fluorouracil on viability of human breast cancer (MCF-7) cell line

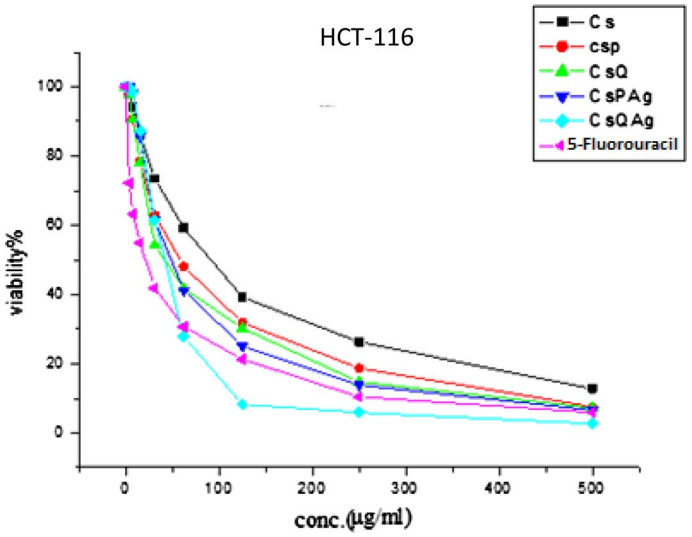

Fig. 12 Effect of concentration (0–500 µg/ml) of compounds **CS**, **CSQ**, **CSP**, **CSQ/Ag**, **CSP/Ag**, and 5-fluorouracil on viability of human colon cancer (HCT-116) cell line

Cytotoxic evaluation

All the new Schiff bases and their nanocomposites **CSQ**, **CSP**, **CSQ/Ag**, and **CSP/Ag** have been investigated in terms of their cytotoxic effects in cancer cells, namely, liver (HepG-2), breast (MCF-7), and colon (HCT-116) by the colorimetric method

Table 1 Cytotoxicity (IC_{50}) of compounds CS, CSQ, CSP, CSQ/Ag, and CSP/Ag against different cancer cell lines

Compounds	HepG-2	MCF-7	HCT-116
Cs	112	137	104
CSQ	102	107	71.7
CSP	86.3	103	58.4
CSQ/Ag	49.8	55.1	41.9
CSP/Ag	70	102	56.7
5-fluorouracil	6.44	28	21.5

as rendered in Figs. 10, 11 and 12. The inhibitory activities of the targetable compounds against tumor cell lines were compared with 5-fluorouracil as a reference drug which showed IC_{50} of 6.44, 28, and 21.5 µg/ml, respectively. Cytotoxic analysis of tested compounds was spotted and estimated by its ability to cause 50% inhibition of cell growth compared to the unprocessed control cells (IC_{50} value), as summarized in Table 1. The antitumor activity profile proposed that the examined compounds exhibited variable activities compared to the reference drug. The newly synthesized chitosan Schiff bases and their nanocomposites have good to moderate antiproliferative activity against the three cancer cell lines. From the displayed results, the IC_{50} values indicated that the compounds had potent growth inhibition against all tested cell lines. Particularly, the cited chitosan Schiff base **CSQ/Ag**, which is bearing with quinolinone ring and loaded with silver nanoparticles, revealed the highest antiproliferative activity toward three cancer cell lines HCT-116, MCF-7, and HePG-2 with minimum IC_{50} values in the range 41.9–55.1 µg/ml compared to chemotherapeutic agent 5-fluorouracil. Compounds **CSQ** and **CSP** have a moderate effect on cancer cells, while the compounds **CSQ/Ag** and **CSP/Ag** displayed good cytotoxic activities toward the three tested cancer cell lines, in addition, compound **CS** alone didn't show significant activity. The presence of heterocyclic scaffolds in chitosan Schiff bases increased the anticancer activities. Chitosan Schiff base with pyranoquinolinone ring system **CSP** has a higher activity than compound **CSQ** with quinolinone ring, with IC_{50} equal to 86.3, 103 and 71.7 µg/ml against HepG-2, MCF-7, and HCT-116, respectively. It has been also noticed that insertion of Ag NPs onto the synthesized Schiff bases played a vital role in the enhancement of growth inhibitory activity. Investigations of the anti-proliferative activity toward HCT-116 cells showed that it is the most sensitive cell line to the influence of the target compounds. The prepared Schiff bases proved to be even more active than the starting chitosan. The IC_{50} outcomes are designed graphically in Fig. 13.

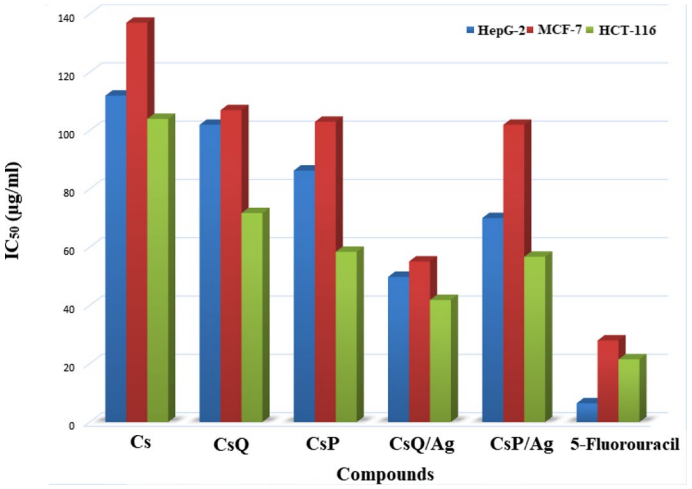

Fig. 13 Virtual IC_{50} values of the target compounds **CS**, **CSQ**, **CSP**, **CSQ/Ag**, **CSP/Ag** and 5-fluorouracil against HepG-2, MCF-7, and HCT-116 cell lines

The effects of the investigational compounds on cell viability and proliferation

Liver cancer cell line HepG-2

The compounds **CS**, **CSQ**, **CSP**, **CSQ/Ag**, and **CSP/Ag** were investigated against human liver cancer cell line HepG-2 for 24 h and compared with a reference drug 5-fluorouracil, using the colorimetric assay. Estimation of viability % of HepG-2 cell line is shown in Fig. 10. Compound **CSQ/Ag** manifested significant growth inhibitory activity against HepG-2 which was more effective than standard drug at concentrations (125, 250, and 500 µg/ml). While titled compounds **CS**, **CSQ**, **CSP**, and **CSP/Ag** were found to be less active than **CSQ/Ag**.

Breast cancer cell line MCF-7

Assessment of viability % of breast cancer cell line (MCF-7) post-treatment with compounds **CS**, **CSQ**, **CSP**, **CSQ/Ag**, and **CSP/Ag** for 24 h related to standard control drug, 5-Fluorouracil, using the colorimetric assay is represented graphically in Fig. 11. Nearly, all the checked compounds exhibited notable inhibitory activity for MCF-7 cells. The results presented that prepared Schiff base **CSQ/Ag** induced remarkable inhibitory activity for MCF-7 cell line than the other tested compounds. In addition, the inhibition % of the cell's viability of compound **CSQ/Ag** was higher than the reference drug at concentrations (125, 250, and 500 µg/ml). Meanwhile, Schiff bases **CSQ**, **CSP**, and **CSP/Ag** were found to be less active in the series.

Colon cancer cell line HCT-116

Exponentially growing colon cancer cells (HCT-116) were treated with **CS**, **CSQ**, **CSP**, **CSQ/Ag**, and **CSP/Ag** for 24 h compared with 5-Fluorouracil using the colorimetric assay (Fig. 12). The tested compounds showed activity comparable to the standard anticancer drug, 5-fluorouracil against HCT-116 cells. The results pointed out that compound **CSQ/Ag** executed remarkable results more than standard reference drug, 5-fluorouracil at concentrations (62.5, 125, 250, and 500 µg/ml). Moreover, the ability to inhibit viability of **CSP/Ag** was close to reference drug at concentrations (125, 250, and 500 µg/ml). In addition, the % inhibition of the cell's viability of Schiff base **CSQ** was very close to positive control at concentrations (250 and 500 µg/ml).

Structure–activity relationship (SAR)

Noteworthy, the structure–activity relationship (SAR) of the aforementioned tested compounds indicates that these compounds mainly depend on their main structural features of presence chitosan attached to heterocyclic rings via azomethine linkage. From all results we got and what was found in the literature, conversion of amino group to azomethine group through Schiff base formation with heterocyclic carboxaldehyde scaffolds enhances the antitumor activity [61–63]. It has been noticed that Schiff base **CSQ** with quinolinone ring (IC_{50} ranged from 71 to 107 µg/ml) has a higher activity than **CS** chitosan itself (IC_{50} ranged from 104 to 137 µg/ml). This may be due to the presence of quinoline analogue which acts as pharmacophoric moiety and azomethine group. Also, chitosan Schiff base bearing pyranoquinolinone ring system **CSP** (IC_{50} ranged from 58 to 103 µg/ml) disclosed better potency against three tumor cells HepG-2, MCF-7, HCT-116 compared to Chitosan itself **CS**.

On the other hand, several prior studies proved that Ag NPs possess therapeutic cancer treatment potential because of their distinctive properties. In cancer cells, series of processes occurs starting with a loss of inner balance and redox state destabilization then Ag^+ produced by oxidation of Ag NPs agglomerated in the cytoplasm and membranes of cells which affects cellular damage and lead to cell death; Oxidative stress induces DNA damage and resulting in cell destruction [64–66]. Regarding the previously mentioned, grafting of silver nanoparticles onto prepared chitosan Schiff bases caused a boosting in the antiproliferative activity against three treated cells. Compound **CSQ/Ag** (IC_{50} ranged from 41 to 55 µg/ml) disclosed better potency toward the cancer cell lines HepG-2, MCF-7, HCT-116 than compound **CSQ** (IC_{50} ranged from 71 to 107 µg/ml). Moreover, compound **CSP/Ag** (IC_{50} ranged from 56 to 102 µg/ml) was significantly more active toward all cell lines compared with **CSP** (IC_{50} ranged from 58 to 103 µg/ml). It was concluded that hybridizing of chitosan with quinolinone and pyranoquinolinone through Schiff bases formation led to enhancement the cytotoxic activity against most tested human cell lines. Interestingly, the acquired results claimed that the incorporation of silver nanoparticles into novel synthesized chitosan Schiff bases reduces the tumor cells.

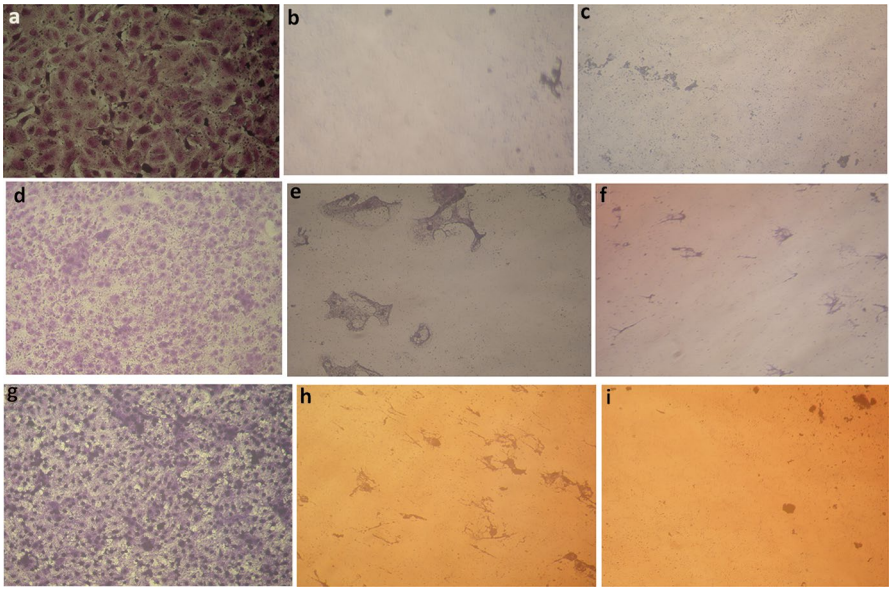

Fig. 14 Morphological changes in **HepG-2** cells incubated for 24 h **a** negative control (untreated) **b** with 250 µg/ml concentration of compound **CSQ/Ag c** with 500 µg/ml concentration of compound **CSQ/Ag**. Morphological changes in **MCF-7** cells incubated for 24 h **d** negative control **e** with 250 µg/ml concentration of compound **CSQ/Ag f** with 500 µg/ml concentration of compound **CSQ/Ag**. Morphological changes in **HCT-116** cells incubated for 24 h **g** negative control **h** with 250 µg/ml concentration of compound **CSQ/Ag i** with 500 µg/ml concentration of compound **CSQ/Ag.** The morphological alterations were microscopically detected at 100×magnification using inverted microscope (CKX41; Olympus, Japan)

Morphological changes in cells were featured on treatment with compounds and microscopic images after using the most powerful compound **CSQ/Ag** are presented in Fig. 14.

Antioxidant activity

It is well known that free radical scavenging activity has received considerable attention owing to its importance in foods and in biological materials. In fact, the free radicals result in biological damages, generally by oxidative processes. This case occurs in autoxidation, lipid peroxidation, and possibly some aspects of aging, radiation damage, chemical carcinogenesis, or other pathological processes. On the other hand, increasing uncontrolled free radical activity might combine with other factors to cause some diseases such as neurodegenerative diseases, heart disease, cancers, heart diseases, acquired immunodeficiency syndrome, and neurological disorder [67]. An antioxidant agent is known as a material that shields a biological target against oxidative degradation. Vitamin C (ascorbic acid) and vitamin E (α-tocopherol) are used as references in the

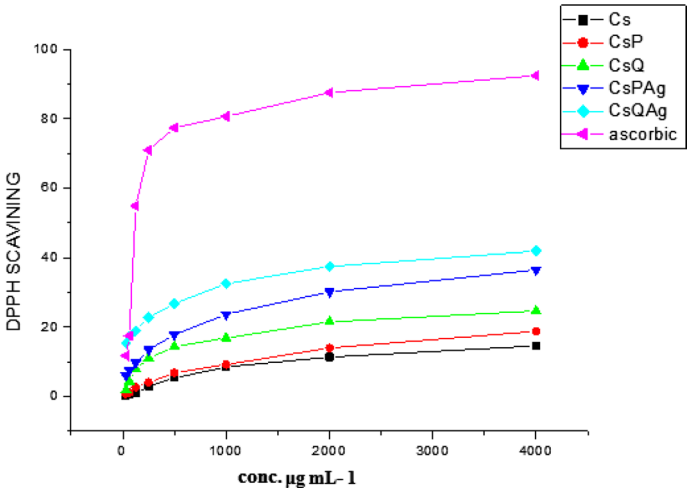

Fig. 15 DPPH-radical scavenging ability of **CSQ**, **CSP**, **CSQ/Ag**, and **CSP/Ag** at different concentrations (31.25–4000 µg mL^{-1})

detection of antioxidant effect of novel examined agents. Antioxidant activity of a compound is known as its ability to scavenge free radicals, which are recognized to be the major factor in the biological damage caused by oxidative stress.

The newly synthesized chitosan Schiff bases **CSQ**, **CSP**, **CSQ/Ag**, and **CSP/Ag** were investigated for their in vitro antioxidant activity showing the scavenging activity of chitosan and its novel Schiff bases for the DPPH radicals (Fig. 15). All samples exhibited DPPH scavenging ability and the concentration of sample influenced the percentage of DPPH. Comparing with the standard control ascorbic acid, all the chitosan Schiff bases **CSP**, **CSQ**, **CSP/Ag**, and **CSQ/Ag** demonstrated moderate DPPH scavenging ability. The compound that showed relatively high antioxidant activity was **CSQ/Ag**. A Significant association could be found between the concentration of the scavenging ability and the percentage of inhibition. This assay provided information that the scavenging activity of chitosan Schiff bases was enhanced compared with that of original chitosan. In our study, compound **CSQ** revealed higher antioxidant activity than chitosan **CS**. In addition, **CSP** is more active than chitosan alone **CS**. This might be due to the phenolic group of quinolinone and pyranoquinolinone rings which are condensed with chitosan to afford the corresponding Schiff base. In numerous studies, original chitosan was investigated as a potential antioxidant agent. The antioxidant activity of chitosan has been associated with its strong hydrogen-donating ability and it was reported that a low molecular weight and a higher concentration have a positive effect on the activity [68]. Moreover, many studies have been carried out aiming to increase the biological activities by chemical modification of chitosan with heterocyclic compounds. Schiff base derivatives of chitosan are one of the important modifications and the newly formed imine groups improve the pharmacological actions of chitosan as antioxidant activities [69, 70].

An enhancement in the antioxidant activity was observed after the functionalization of chitosan Schiff bases **CSQ** and **CSP** with Ag NPs. It has been remarked that Compound **CSQ/Ag** is more active than **CSQ**. Compound **CSP/Ag** possesses higher antioxidant activity compared with **CSP**. The result obtained in this study was confirmed by the results given in the literature regarding the role of silver nanoparticles in increasing the DPPH radical-scavenging activity [71].

Conclusion

In this paper, novel chemically modified chitosan Schiff bases bearing quinolinone and pyranoquinolinone rings were synthesized. The decoration of new chitosan Schiff bases with silver nanoparticles was then happened to obtain novel nanocomposite. Characterization using spectral and surface analyses techniques was performed, showing evidence for their formation. The cytotoxic activity of the investigated compounds against the three tested cell lines indicated that chitosan Schiff bases disclosed better anticancer activities than chitosan itself. Furthermore, the effect of novel Schiff bases moieties on their antioxidant activity was examined by using the DPPH radical scavenging assay. Therefore, an improvement in the antioxidant activity was noticed after the functionalization of chitosan with quinolinone and pyranoquinolinone which are valuable scaffolds in medicinal chemistry. Interestingly, the incorporation of silver nanoparticles into the newly tested chitosan Schiff bases enhanced their anti-proliferative and antioxidant activity. As a result, Compound **CSQ/Ag** displayed to be the most potent in the two biological studies compared to the references.

Material and methods

Chemistry

Chitosan (Sigma Aldrich), glacial acetic acid (Fisher scientific), triethyl orthoformate (Merck), Remazol red (RB-133), sodium hydroxide, sodium chloride and hydrochloric acid were purchased from Sinopharm Chemical Reagent Company Limited. The used reagents were of analytical grade as received. Distilled water was consumed in all preparations.

Synthesis of chitosan Schiff bases

Compound **P** [72], **Q** [73], and **CsP** [46] was synthesized according to the reported literature methods. Then Chitosan (1 mol) was dissolved in 100 ml acetic acid 5% and stirred at 50 °C for 4 h, and the aldehyde (1 mol) was dissolved in the least amount of ethanol, then the aldehyde solution was added dropwise to the chitosan solution; the reaction mixture was stirred at 70 °C for 24 h. An Orange gel was

formed and collected by filtration, washed several times with a mixture of ethanol and acetone to remove any unreacted materials, dried to give chitosan Schiff bases as powder compounds.

Synthesis of chitosan Schiff bases/Ag NPs composites

Firstly, Ag NPs were prepared as follows: the solution of $AgNO_3$ (0.3 g/10 mL deionized H_2O) was added dropwise to an aqueous solution of sodium borohydride (2.9 M, 6.6 mL) which contains 1 mL of NaOH (0.001 M) and kept under stirring at 70 °C for 60 min. The color of the colloidal solution was turned to yellow color by the addition of $AgNO_3$. Secondly, chitosan Schiff bases loaded with Ag NPs were prepared using Ag NPs with a weight ratio of (1%) of nano-materials with respect to chitosan Schiff bases. Ag NPs were dispersed individually in ethanol by sonication for 20 min then it was added dropwise to the previously prepared Schiff bases solution under stirring for 6 h. The composite was precipitated in a mixture of acetone and ethanol, filtered, and finally dried in air.

Physicochemical characterization of chitosan Schiff bases.

FTIR analysis

Fourier transform infrared (FT-IR) measurements were accomplished using FT-IR (Thermo electron corporation Nicolet avatar 370 CSL) with the wavenumber range 500–4000 cm^{-1} in the Training section—ministry of military production.

X-ray diffraction

X-ray diffractograms of chitosan and chitosan Schiff base samples were carried out using ARL™ X'TRA Powder Diffractometer (Thermo Fisher Scientific Inc.) with Cu-K-alpha wavelength = 1.540598 $Å^{o}$A and current 44 mA–voltage 45 kV.

Scanning electron microscope (SEM)

The chitosan Schiff base sample was analyzed using an SEM model Quanta 250 field emission gun (FEG) attached to an energy dispersive X-ray (EDX) analysis unit with 30 K.V. accelerating voltage, 14 × up to 1,000,000 magnification and Gun.1n resolution).

Thermal gravimetric analysis (TGA)

The sample was carried out by Q500TA instruments.

Biological evaluation

Reagents and chemicals

Dimethyl sulfoxide (DMSO), (1%) crystal violet stain (It is composed of 0.5% (w/v) crystal violet and 50% methanol then made up to volume with dd H_2O and was filtered using a Whatman No.1 filter paper) and trypan blue dye were purchased from Sigma (St. Louis, Mo., USA). Additionally, Fetal Bovine serum, RPMI 1640, DMEM, HEPES buffer solution, gentamycin, L-glutamine and 0.25% Trypsin-EDTA were acquired from Lonza.

Cell lines and Cell culture

Human Hepatocellular carcinoma cells (**HepG-2)**, colon carcinoma cells (**HCT-116)** and breast carcinoma cells (**MCF-7)** were obtained from VACSERA Tissue Culture Unit. All cancer cell lines were preserved at 37 °C in a humidified atmosphere with 5% CO_2 in Dulbecco's modified Eagle's medium (DMEM) supplemented with 10% heat-inactivated fetal bovine serum, 1% L-glutamine, HEPES buffer and 50 µg/ml gentamycin and were sub-cultured two times a week.

Cytotoxicity evaluation using viability assay

The cells were seeded in 96-well plate at concentration of 1×10^4 cells per well in 100 µl of growth medium. After 24 h of seeding freshly medium including several concentrations of the tested samples was added. Serial two-fold dilutions of the examined chemical compound were added to confluent cell monolayers operated into 96-well, flat-bottomed microtiter plates (Falcon NJ, USA) using a multichannel pipette. The microtiter plates were incubated at 37ºC in a humidified incubator with 5% CO_2 for extent of 48 h. Three wells were utilized for each concentration of the test sample. Control cells were incubated without examined sample and with or without DMSO. The small percentage of DMSO present in the wells (maximal 0.1%) was found not to affect the experiment. After incubation of the cells for at 37 °C, various concentrations of samples were added, and the incubation remained for 24 h and viable cells yield was established by a colorimetric method [74, 75]. In brief, when incubation period was ended, media were extracted, and the crystal violet solution (1%) was added to each well for 30 min. The stain was isolated, and the plates were rinsed using tap water until all excess stain was removed. As well, 30% of Glacial acetic acid was added to all wells and perfectly mixed, then the absorbance of the plates was measured after shaking well on Microplate reader (TECAN, Inc.), with a wavelength of 490 nm. All outcomes were rectified for background absorbance recognized in wells without addition of stain. Treated samples were correlated with the cell control in the absence of the examined compounds. All experiments were carried out in triplicate. The cytotoxicity of each examined compound was calculated. Optical

density was assessed with the microplate reader (SunRise, TECAN, Inc., USA) to decide the number of viable cells and the percentage of viability was calculated as [(ODt/ODc)] × 100% where ODt is the mean optical density of wells treated with the examined sample and ODc is the mean optical density of untreated cells. The relation between surviving cells and drug concentration is plotted in a graph to obtain the survival curve of each cancer cell line after treatment with the characteristic compound. The concentration necessary to induce toxic effects in 50% (IC_{50}) of intact cells, was determined from graph of the dose response curve for each concentration by using Graph pad Prism software (San Diego, CA. USA).

Antioxidant assay

The antioxidant activity of extract was carried out at the Regional Center for Mycology and Biotechnology (RCMB) et al.-Azhar University by the DPPH free radical scavenging assay in triplicate and average values were measured.

DPPH radical scavenging activity

Freshly prepared (0.004%w/v) methanol solution of 2,2-diphenyl-1 picrylhydrazyl (DPPH) radical was prepared and stored at 10 °C in the dark. The methanol solution of the examined compound was prepared. An aliquot of 40 uL from the methanol solution was added to 3 ml of DPPH solution. Absorbance measurements were noted immediately with a UV–visible spectrophotometer (Milton Roy, Spectronic 1201). The absorbance decreasing at 515 nm was determined constantly, with data being noted at 1 min intervals until the absorbance stabilized (16 min). The DPPH radical absorbance without antioxidant (reference) and the control compound ascorbic acid were also measured. All the determinations were executed in three replicates and averaged. The percentage inhibition (PI) of the DPPH radical was worked out according to the formula:

$$\mathrm{PI} = \left[\{(\mathrm{AC} - \mathrm{AT})/\ \mathrm{AC}\}\ \mathrm{x}\ 100\right] \quad (1)$$

where AC = Absorbance of the control at t = 0 min and AT = absorbance of the sample + DPPH at t = 16 min [76].

Funding Open access funding provided by The Science, Technology & Innovation Funding Authority (STDF) in cooperation with The Egyptian Knowledge Bank (EKB).

Declarations

Conflict of interest The authors declare no competing interests.

References

1. Zivanovic S, Li J, Davidson PM, Kit K (2007) Physical, mechanical, and antibacterial properties of Chitosan/PEO blend films. Biomacromolecules 8:1505–1510
2. Ngwuluka NC, Abu-Thabit NY, Uwaezuoke OJ, Erebor JO, Ilomuanya MO, Mohamed RR, Soliman SM, Elella MHA, Ebrahim NA (2021) Natural polymers in micro-and nanoencapsulation for therapeutic and diagnostic applications part II-polysaccharides and proteins. In: Nano- and microencapsulation - techniques and applications, pp 55. https://doi.org/10.5772/intechopen.95402
3. Ngwuluka NC, Abu-Thabit NY, Uwaezuoke OJ, Erebor JO, Ilomuanya MO, Mohamed RR, Soliman SM, Elella MHA, Ebrahim NA (2020) Natural polymers in micro-and nanoencapsulation for therapeutic and diagnostic applications: part I: lipids and fabrication techniques. In: Nano- and microencapsulation - techniques and applications. https://doi.org/10.5772/intechopen.94856
4. Elella MHA, Hanna DH, Mohamed RR, Sabaa MW (2021) Synthesis of xanthan gum/trimethyl chitosan interpolyelectrolyte complex as pH-sensitive protein carrier. Polym Bull. https://doi.org/10.1007/s00289-021-03656-3
5. Elella MHA, Sabaa M, Hanna DH, Abdel-Aziz MM, Mohamed RR (2020) Antimicrobial pH-sensitive protein carrier based on modified xanthan gum. J Drug Deliv Sci Technol 57:101673
6. Ali SS, Kenawy ER, Sonbol FI, Sun J, Al-Etewy M, Ali A, Huizi L, El-Zawawy NA (2019) Pharmaceutical potential of a novel chitosan derivative schiff base with special reference to antibacterial, anti-biofilm, antioxidant, anti-inflammatory. Hemocompat Cytotox Act Pharm Res 36(1):5
7. Elella MHA, Abdel-Aziz MM, Abd El-Ghany NA (2021) Synthesis of a high-performance antimicrobial o-quaternized alginate–a promising potential antimicrobial agent. Cellul Chem Technol 55:75–86
8. Adhikari HS, Yadav PN (2018) Anticancer activity of chitosan, chitosan derivatives, and their mechanism of action. Int J Biomater 2018:1–29
9. Dutta PK, Tripathi S, Mehrotra GK, Dutta J (2009) Perspectives for chitosan based antimicrobial films in food applications. Food Chem 114:1173–1182
10. Kim S (2018) Competitive biological activities of chitosan and its derivatives: antimicrobial, antioxidant, anticancer, and anti-inflammatory activities. Int J Polym Sci 2018:1–13
11. Soni B, Mahmoud B, Chang S, El-Giar EM, Hassan E (2018) Physicochemical, antimicrobial and antioxidant properties of chitosan/TEMPO biocomposite packaging films. Food Packag Shelf Life 17:73–79
12. Phanindrudu MS, Wakade B, Tiwari DK, Likhar PR, Tiwari DK (2018) Transition-metal-free approach for the synthesis of 4-Aryl-quinolines from alkynes and anilines. J Org Chem 83:9137–9143
13. Wakade SB, Tiwari DK, Ganesh PSP, Phanindrudu M, Likhar PR, Tiwari DK (2017) Transition-metal-free quinoline synthesis from acetophenones and anthranils via sequential one-carbon homologation/conjugate addition/annulation cascade. Org lett 19:4948
14. Upadhyay KD, Dodia NM, Khunt RC, Chaniara RS, Shah AK (2018) Synthesis and biological screening of pyrano[3,2-c]quinolone analogues as anti-inflammatory and anticancer agents. ACS Med Chem Lett 9(3):283–288
15. Chen IS, Wu SJ, Tsai IL, Wu TS, Pezzuto JM, Lu MC, Chai H, Suh N, Teng CM (1994) Chemical and bioactive constituents from Zanthoxylum simulans. J Nat Prod 57:1206
16. Arasakumar T, Mathusalini S, Gopalan S, Shyamsivappan S, Ata A, Mohan PS (2017) Biologically active perspective synthesis of heteroannulated 8-nitroquinolines with green chemistry approach. Bioorg Med Chem Lett 27:1538–1546

17. Likhitwitayawuid K, Angerhofer C, Cordell G, Pezzuto J, Ruangrungsi N (1993) Cytotoxic and antimalarial bisbenzylisoquinoline alkaloids from Stephania erecta. J Nat Prod 56(1):30–38
18. Hassanin HM, Abd Elmoneam WR, Mostafa MA (2019) Synthesis and antitumor activity evaluation of different 2,5-dialkyloxazolopyrano[3,2-*c*]quinolinone derivatives. Med Chem Res 28:28–38
19. Othman ES, Hassan H, Abass M (2019) Some new pyrano[3,2-*c*]quinoline-3-carboxamides and their antioxidant activity. J Heterocycl Chem 56:3257–3266
20. Jadhav S, Patil R, Kumbhar D, Patravale A, Chandam D, Deshmukh M (2015) DABCO promoted one pot efficient synthesis and antioxidant activity of 2-amino-4-phenyl-5-oxo-5,6-dihydro-4H-pyrano[3,2-c]quinoline-3-carbonitrile derivatives. Int J Pharm Sci Rev Res 35(2):75–82
21. Karthikeyan MS, Prasad DJ (2006) Synthesis and biological activity of Schiff and Mannich bases bearing 2,4-dichloro-5-fluorophenyl moiety. Bioorg Med Chem 14:7482
22. Bensaber SM, Allafe HA, Ermeli NB, Mohamed SB, Zetrini AA, Alsabri SG, Erhuma M, Hermann A, Jaeda MI, Gbaj AM (2014) Chemical synthesis, molecular modelling, and evaluation of anticancer activity of some pyrazol-3-one Schiff base derivatives. Med Chem Res 23:5120–5134
23. Eltayeb NE, Lasri J, Soliman SM, Mavromatis C, Hajjar D, Elsilk SE, Babgi BA, Hussien MA (2020) Crystal structure, DFT, antimicrobial, anticancer and molecular docking of (4*E*)-4-((aryl) methyleneamino)-1,2-dihydro-2,3-dimethyl-1-phenylpyrazol-5-one. J Mol Struct 1213:128185
24. Fayed EA, Eldin RRE, Mehany A, Bayoumi AH, Ammar YA (2021) Isatin-Schiff's base and chalcone hybrids as chemically apoptotic inducers and EGFR inhibitors; design, synthesis, anti-proliferative activities and in silico evaluation. J Mol Struct 1234:130159
25. Kumar M, Padmini T, Ponnuvel K (2017) Synthesis, characterization, and antioxidant activities of Schiff bases are of cholesterol. J Saudi Chem Soc 21:S322–S328
26. Shahraki S, Heidari M, Heydari A (2019) Novel tetradentate Schiff base zinc (II) complex as a potential antioxidant and cancer chemotherapeutic agent: insights from the photophysical and computational approach. J Mol Struct 1177:536–544
27. Hassanin HM, Serya RAT, Abd Elmoneam WR, Mostafa MA (2018) Synthesis and molecular docking studies of some novel Schiff bases incorporating 6-butylquinolinedione moiety as potential topoisomerase IIβ inhibitors. Soc Open Sci 5:172407
28. Elshaarawy RFM, Refaee AA, El-Sawi EA (2016) Pharmacological performance of novel poly-(ionicliquid)-grafted chitosan-N-salicylidene Schiff bases and their complexes. Carbohydr Polym 146:376–387
29. Khalil AM, Abdel-Monem RA, Osama MD, Hashim AI, Nada A, Rabie ST (2017) Synthesis, characterization, and evaluation of antimicrobial activities of chitosan and carboxymethyl chitosan schiff-base/silver nanoparticles. J Chem 2017:1–11
30. Elella MHA, Goda ES, Gab-Allah MA, Hong SE, Pandit B, Lee S, Gamal H, urRehman A, Yoon KR (2020) Xanthan gum-derived materials for applications in environment and eco-friendly materials: a review. J Environ Chem Eng 9:104702
31. Lee J, Goda ES, Choi J, Park J, Lee S (2020) Synthesis and characterization of elution behavior of nonspherical gold nanoparticles in asymmetrical flow field-flow fractionation (AsFlFFF). J Nanopart Res 22(9):1–2
32. Elella MHA, Goda ES, Gamal H, El-Bahy SM, Nour MA, Yoon KR (2021) Green antimicrobial adsorbent containing grafted xanthan gum/SiO2 nanocomposites for malachite green dye. Int J Biol Macromol 191:385–395
33. Elella MHA, Goda ES, Abdallah HM, Shalan AE, Gamal H, Yoon KR (2021) Innovative bactericidal adsorbents containing modified xanthan gum/montmorillonite nanocomposites for wastewater treatment. Int J Biol Macromol 167:1113–1125
34. Pandit B, Goda ES, Elella MH, urRehman A, Hong SE, Rondiya SR, Barkataki P, Shaikh SF, Al-Enizi AM, El-Bahy SM, Yoon KR (2022) One-pot hydrothermal preparation of hierarchical manganese oxide nanorods for high-performance symmetric supercapacitors. J Energy Chem 65:116–126
35. Mittal AK, Kumar S, Banerjee UC (2014) Quercetin and gallic acid mediated synthesis of bimetallic (Ag-Se) nanoparticles and their antitumor and antimicrobial potential. J Colloid Interface Sci 431:194–199
36. Lin J, Huang Z, Wu H, Zhou W, Jin P, Wei P (2014) Inhibition of autophagy enhances the anticancer activity of silver nanoparticles. Autophagy 10(11):2006–2020
37. Goda ES, Elella MHA, Sohail M, Singu BS, Pandit B, El Shafey AM, Aboraia AM, Gamal H, Hong SE, Yoon KR (2021) N-methylene phosphonic acid chitosan/graphene sheets decorated with silver nanoparticles as green antimicrobial agents. Int J Biol Macromol 182:680–688

38. Goda ES, Elella MHA, Hong SE, Pandit B, Yoon KR, Gamal H (2021) Smart flame retardant coating containing carboxymethyl chitosan nanoparticles decorated graphene for obtaining multifunctional textiles. Cellulose 28(8):5087–5105
39. Elella MHA, Goda ES, Yoon KR, Hong SE, Morsy MS, Sadak RA, Gamal H (2021) Novel vapor polymerization for integrating flame retardant textile with multifunctional properties. Compos Commun 24:100614
40. Abdel-Aziz MM, Elella MHA, Mohamed RR (2020) Green synthesis of quaternized chitosan/silver nanocomposites for targeting mycobacterium tuberculosis and lung carcinoma cells (A-549). Int J Biol Macromol 142:244–253
41. Venkatesan J, Lee J-Y, Kang DS, Anil S, Kim S-K, Shim MS, Kim DG (2017) Antimicrobial and anticancer activities of porous chitosan-alginate biosynthesized silver nanoparticles. Int J Biol Macromol 98:515–525
42. Suman TY, Rajasree SR, Ramkumar R, Rajthilak C, Perumal P (2014) The Green synthesis of gold nanoparticles using an aqueous root extract of Morinda citrifolia L. Spectrochim Acta A Mol Biomol Spectrosc 118:11–16
43. Shareef JU, Rani MN, Anand S, Rangappa D (2017) Synthesis and characterization of silver nanoparticles from Penicillium sps. Mater Today 4(11):11923–11932
44. Vijayashree IS, Niranjana P, Prabhu G, Sureshbabu VV, Manjanna J (2017) Conjugation of Au nanoparticles with chlorambucil for improved anticancer activity. J Clust Sci 28(1):133–148
45. Banu A, Gousuddin M, Yahya EB (2021) Green synthesized monodispersed silver nanoparticles' characterization and their efficacy against cancer cells. Biomed Res Ther 8(8):4476–4482
46. Ibrahim SM, Hassanin HM, Abdelrazek MM (2020) Synthesis, and characterization of chitosan bearing pyranoquinolinone moiety for textile dye adsorption from wastewater. Water Sci Technol 81(3):421–435
47. Xiaoxiao J, Jiangtao W, Jie B (2009) Synthesis and antimicrobial activity of the Schiff base from chitosan and citral. Carbohydr Res 344:825–829
48. Sashikala S, Shafi SS (2014) Synthesis and characterization of chitosan Schiff base derivatives. Sch Res J 6(2):90–97
49. Wang Z, Xu C, Zhao M, Zhao C (2014) One-pot synthesis of narrowly distributed silver nanoparticles using phenolic-hydroxyl modified chitosan and their antimicrobial activity. RSC Adv 4(87):47021–47030
50. Elshaarawy RF, Seif GA, El-Naggar ME, Mostafa TB, El-Sawi EA (2019) In-situ and ex-situ synthesis of poly-(imidazolium vanillyl)-grafted chitosan/silver nanobiocomposites for safe antibacterial finishing of cotton fabrics. Eur Polym J 116:210–221
51. Baran T, Açıksöz E, Menteş A (2016) Highly efficient, quick and green synthesis of biarlys with chitosan supported catalyst using microwave irradiation in the absence of solvent. Carbohydr Polym 142:189–198
52. Wang X, Du Y, Fan L, Liu H, Hu Y (2005) Chitosan- metal complexes as antimicrobial agent: synthesis, characterization and Structure-activity study. Polym Bull 55:105–113
53. Salama HE, Saad GR, Sabaa MW (2015) Synthesis, characterization and biological activity of Schiff bases based on chitosan and arylpyrazole moiety. Int J Biol Macromol 79:996–1003
54. Kenawy E, Ali SS, Al-Etewy M, Sun J, Wu J, El-Zawawy N (2019) Synthesis, characterization and biomedical applications of a novel Schiff base on methyl acrylate functionalized chitosan bearing pnitrobenzaldehyde groups. Int J Biol Macromol 122:833–843
55. Hajji S, Salem RBS, Hamdi M, Jellouli K, Ayadi W, Nasri M, Boufi S (2017) Nanocomposite films based on chitosan–poly(vinyl alcohol) and silver nanoparticles with high antibacterial and antioxidant activities. Process Saf Environ Prot 111:112–121
56. Abdel-Monem RA, Khalil AM, Darwesh Osama M, Hashim AI, Rabie ST (2020) Antibacterial properties of carboxymethyl chitosan Schiff-base nanocomposites loaded with silver nanoparticles. J Macromol Sci A 57:145–155
57. Mohammadi A, Doctorsafaei AH, Burujeny SB, Rudbari HA, Kordestani N, Najafabadi SAA (2020) Silver(I) complex with a Schiff base ligand extended waterborne polyurethane: A developed strategy to obtain a highly stable antibacterial dispersion impregnated with in situ formed silver nanoparticles. Chem Eng Sci 381:122776
58. Kumar S, Kumari M, Dutta PK, Koh J (2014) Chitosan biopolymer schiff base: preparation, characterization, optical and antibacterial activity. Int J Polym Mater 63:173–177
59. Ma H, Kong A, Ji Y, He B, Song Y, Li J (2019) Ultrahigh adsorption capacities for anionic and cationic dyes from wastewater using only chitosan. J Clean Prod 214:89–94

60. Amtul JS, Yasha NB, Sitara N (2018) Elimination of a carcinogenic anionic dye congo red from water using hydrogels based on chitosan, acrylamide and graphene oxide. J Bioprocess Biotech 8:2155–9821
61. El-Naggar MM, Haneen DSA, Mehany ABM, Khalil MT (2020) New synthetic chitosan hybrids bearing some heterocyclic moieties with potential activity as anticancer and apoptosis inducers. Int J Biol Macromol 150:1323–1330
62. Shukla S, Srivastava RS, Shrivastava SK, Sodhi A, Kumar P (2013) Synthesis, characterization, in vitro anticancer activity, and docking of Schiff bases of 4-amino-1,2-naphthoquinone. Med Chem Res 22:1604–1617
63. Kamel MM, Ali HI, Anwar MM, Mohamed NA, Soliman AM (2010) Synthesis, antitumor activity and molecular docking study of novel Sulfonamide-Schiff's bases, thiazolidinones, benzothiazinones and their C-nucleoside derivatives. Eur J Med Chem 45:572–580
64. Priya K, Kumar M, Janani B (2020) Chitosan-mediated synthesis of biogenic silver nanoparticles (AgNPs), nanoparticle characterisation and in vitro assessment of anticancer activity in human hepatocellular carcinoma HepG2 cells. Int J Biol Macromol 149:844–852
65. Vivek R, Ramar T, Krinasamy M, Gunasekaran P, Kaveri K, Kannan S (2012) Green biosynthesis of silver nanoparticles from Annona squamosa leaf extract and its in vitro cytotoxic effect on MCF-7 cells. Process Biochem 47:2405–2410
66. Takahashi A, Masuda A, Sun M, Centonze VE, Herman B (2004) Oxidative stress-induced apoptosis is associated with alterations in mitochondrial caspase activity and Bcl-2-dependent alterations in mitochondrial pH (pHm). Brain Res Bull 62(6):497–504
67. Hajji S, Khedir SB, Hamza-Mnif I, Hamdi M, Jedidi I, Kallel R, Boufi S (1863) Nasri M (2019) Biomedical potential of chitosan-silver nanoparticles with special reference to antioxidant, antibacterial, hemolytic and in vivo cutaneous wound healing effects. Biochim Biophys Acta Gen Subj 1:241–254
68. Vinsova J, Vavrikova E (2011) Chitosan derivatives with antimicrobial: antitumor and antioxidant activities −a review. Curr Pharm Des 17:3596–3607
69. Demetgül C, Beyazit N (2018) Synthesis, characterization and antioxidant activity of chitosan-chromone derivatives. Carbohydr Polym 181:812–817
70. Beyazit N, Çakran HS, Cabir A, Akışcan Y, Demetgül C (2020) Synthesis, characterization and antioxidant activity of chitosan Schiff base derivatives bearing (−)-gossypol. Carbohydr Polym 240:116333
71. Li Q, Wei L, Zhang J, Gu G, Guo Z (2019) Significantly enhanced antioxidant activity of chitosan through chemical modification with coumarins. Polym Chem 10:1480–1488
72. Othman ES, Hassanin HM, Mostafa MA (2019) Synthesis of Pyrano[3,2-c]quinoline-3-carboxaldehyde and 3- (Ethoxymethylene) –pyrano [3,2-c] quinolinone and Their Chemical Behavior toward Some Nitrogen and Carbon Nucleophiles. J Heterocycl Chem 56:1598–1604
73. Tomita K (1951) The Antibacterial properties of compounds containing the tricarbonyl-methane group. V the syntheses of 3-Acyl-2, 4-dihydroxyquinolines and of the related compounds, with respect to their antibacterial properties Yakugaku Zasshi. J Pharm Soc Japan 71(10):1100–1112
74. Mosmann T (1983) Rapid colorimetric assay for cellular growth and survival: application to proliferation and cytotoxicity assays. J Immunol Methods 65:55–63
75. Gomha SM, Riyadh SM, Mahmmoud EA, Elaasser MM (2015) Synthesis and anticancer activities of thiazoles, 1,3-thiazines, and thiazolidine using chitosan-grafted- poly(vinylpyridine) as basic catalyst. Heterocycles 91(6):1227–1243
76. Yen GC, Duh PD (1994) Scavenging effect of methanolic extracts of peanut hulls on free radical and active oxygen species. J Agric Food Chem 42:629–632